# Current-induced motion and pinning of domain walls in spin-valve nanowires studied by XMCD-PEEM

V. Uhlíř,[1,2,*] S. Pizzini,[1] N. Rougemaille,[1] J. Novotný,[3] V. Cros,[4] E. Jiménez,[5] G. Faini,[6] L. Heyne,[7] F. Sirotti,[8] C. Tieg,[9] A. Bendounan,[8,10] F. Maccherozzi,[8,10] R. Belkhou,[8,10] J. Grollier,[4] A. Anane,[4] and J. Vogel[1]

[1]*Institut Néel, CNRS and UJF, BP 166, 38042 Grenoble, France*

[2]*Institute of Physical Engineering, Brno University of Technology, 61669 Brno, Czech Republic*

[3]*Institute of Mathematical Engineering, Brno University of Technology, 61669 Brno, Czech Republic*

[4]*Unité Mixte de Physique CNRS/Thales and Université Paris Sud 11, 91767 Palaiseau, France*

[5]*Depto. Física de la Materia Condensada and Inst. Nicolás Cabrera, Universidad Autónoma de Madrid, 28049 Madrid, Spain*

[6]*PhyNano Team, Laboratoire de Photonique et de Nanostructures, CNRS, route de Nozay, 91460 Marcoussis, France*

[7]*Fachbereich Physik, Universität Konstanz, Universitätsstr. 10, 78457 Konstanz, Germany*

[8]*Synchrotron SOLEIL, L'Orme des Merisiers, Saint-Aubin, 91192 Gif-sur-Yvette, France*

[9]*European Synchrotron Radiation Facility, BP 200, 38043 Grenoble, France*

[10]*ELETTRA, Sincrotrone Trieste, Basovizza, 34012 Trieste, Italy*

(Received 15 March 2010; published 11 June 2010)

Very large average velocities, up to 600 m/s, have been found for domain-wall motion driven by 3-ns-long pulses of electric current in zero magnetic field in the NiFe layer of 200-nm-wide NiFe/Cu/Co nanowires. For longer pulses, the domain-wall motion is strongly hindered by pinning potentials. Dipolar interactions between the NiFe and Co layers caused by anisotropy inhomogeneities have been identified as the most important among the different potential sources of DW pinning. The domain-wall velocities increase with current density, but a substantial drop is observed at current densities above $4\times10^{11}$ A/m$^2$.

DOI: 10.1103/PhysRevB.81.224418 PACS number(s): 75.60.Ch, 72.25.Ba, 85.75.−d, 75.75.−c

## I. INTRODUCTION

The possibility of moving magnetic domain walls (DWs) using spin-polarized currents rather than magnetic fields has recently attracted a considerable interest both from an applied and a fundamental viewpoint.[1,2] Besides the promise of novel efficient electronic devices based on spin-transfer torque (STT), such as magnetic memories, shift registers, or logic devices,[3,4] current-induced DW motion represents a unique fundamental means to investigate the mutual interaction of magnetization and electric current. The effect of electric current on a DW was predicted and tested already in the 1970s,[5] but because of the high-current densities needed for DW motion, the first experimental studies were carried out more than 20 years later,[6] when the evolution of lithography techniques allowed narrow nanowires to be produced.

Considerable progress in the understanding of the phenomenon has been made recently and it is now accepted that the current-driven dynamics of a DW can be described by the Landau-Lifshitz-Gilbert equation to which two components of the STT, adiabatic and nonadiabatic STT terms, are added.[7–9] It has been demonstrated that only the nonadiabatic term is responsible for the long-range DW displacements, of the order of microns, that have been observed using nanosecond current pulses.[10,11]

For a successful implementation of STT in the writing process of spintronic devices, further optimization of systems featuring current-induced DW motion (CIDWM) has to be performed. A major concern is to further reduce the critical-current densities for CIDWM which are presently on the order of $1\times10^{12}$ A/m$^2$ for NiFe.[12] This might be done through an improvement of the STT efficiency. DW velocities have to be increased to reach several hundreds of meter per second.[3] Finally, to assure a reproducible and reliable DW motion, pinning of DWs along the nanowires has to be controlled much more accurately.

Most studies on CIDWM were carried out on single NiFe nanowires with in-plane magnetic anisotropy (for a review see Ref. 2), for which DW displacements with velocities ranging from 1 m/s (Refs. 13 and 14) to 110 m/s (Ref. 15) were found, for current densities in the order of $10^{12}$ A/m$^2$ in zero applied magnetic field. Recent measurements show that systems with perpendicular magnetic anisotropy[10] can feature very high DW velocities (up to 130 m/s) for similar current densities. Similarly to field-induced DW motion, current-induced DW motion for high-current densities is limited by the onset of periodical transformations of the internal DW structure (from transverse to vortex wall and back),[13] occurring beyond the so-called Walker breakdown.[9,16]

Evidence of CIDWM at much lower current densities ($8\times10^{10}$ A/m$^2$) has been first given by Grollier *et al.*[17] for the NiFe layer of spin-valve NiFe/Cu/Co nanowires. The critical-current density could be further lowered to $1\times10^{10}$ A/m$^2$ by employing CoFeB as a soft magnetic layer instead of NiFe.[18] In similar devices, it was then observed that for short current pulses ranging from 200 ps to 2 ns, the DW displacement was almost independent of the current-pulse duration, leading to surprisingly large DW velocities.[19] Another unclarified feature of this system was the apparent change in direction of the DW motion on injection of a larger current density. The results presented in this paper will allow to partly explain these observations.

Our recent measurements on similar NiFe/Cu/Co nanowires gave direct microscopic evidence for DW velocities above 180 m/s for current densities as low as $5\times10^{11}$ A/m$^2$.[11] This reduction in the current densities com-

 

pared to single NiFe systems might be partly due to vertical spin currents caused by local-spin accumulation in the DW region. The pure vertical injection of a spin-polarized current has been theoretically predicted[20] to yield a larger efficiency for spin-transfer-induced DW motion. This has been recently confirmed, using transport measurements, for perpendicular current injection in NiFe/Cu/CoFe spin-valve nanowires.[21]

The low critical-current densities and the high DW velocities found for spin-valve nanowires make these systems interesting candidates for spintronic applications. However, one challenge still has to be faced and solved in order to obtain an efficient CIDWM applicable to electronic devices. In this system, as in many other systems reported in literature recently, DW motion has been found to be strongly hindered by pinning potentials.[11,22–25] Improving material quality seems thus to be essential for future developments.

Our objective in this paper is to detect and analyze the DW propagation in the NiFe layer of NiFe/Cu/Co SV nanowires by photoemission electron microscopy combined with x-ray magnetic circular dichroism (XMCD-PEEM). As we will demonstrate, the direct observation of DW movement by magnetic microscopy brings substantial information complementary to transport measurements previously carried out on similar samples.[17–19] The extensive study that we present here gives insight into the average behavior of the system since we compare the action of current pulses of several amplitudes and durations on a multitude of DWs pinned on different pinning sites. We will show that the DW displacements are, in general, not proportional to the current-pulse length, because of the impact of pinning potentials on the DW dynamics. This complicates the accurate determination of DW velocities in NiFe. In the following sections, we will present and discuss the analysis of the distributions of DW displacements and velocities observed in the NiFe layer of our SV devices, before discussing the possible physical reasons for the strong DW pinning.

## II. EXPERIMENTAL

Spin-valve trilayers with the composition Cu 3 nm/NiFe 5 nm/Cu 8 nm/Co 7 nm/CoO 3 nm/Si (100) were deposited by dc magnetron sputtering. The incorporation of a thin CoO layer allows one to increase the coercive field of the Co layer by improving the structure growth. Zigzag-shaped nanowires of widths 200 and 300 nm (see Fig. 1) were obtained using electron-beam lithography combined with lift-off techniques. Top electrodes made of Ti/Au are subsequently fabricated by a second lift-off step. Unless stated otherwise, the images and the results on DW movements shown in this paper refer to 200-nm-wide nanowires.

Micromagnetic simulations were carried out to determine the phase diagram of the DW structure in the NiFe layer of the NiFe/Cu/Co nanowire, as a function of the nanowire width and NiFe thickness.[26] For 200-nm- and 300-nm-wide nanowires with a NiFe thickness of 5 nm, transverse walls (TWs) have lower energy than vortex walls (VW). In comparison to single NiFe nanowires,[27] the borderline between TW and VW stability regions is shifted in favor of TWs due to magnetostatic interaction between NiFe and Co magnetizations.

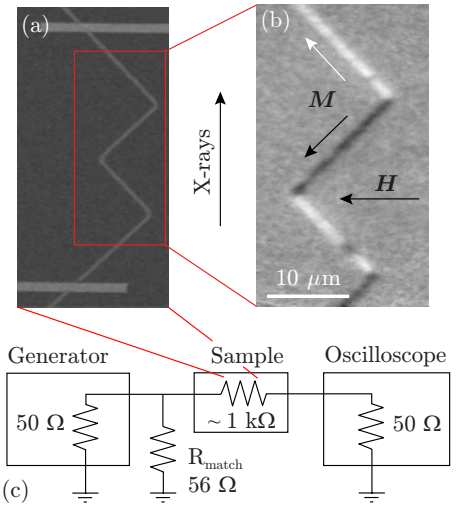


FIG. 1. (Color online) (a) Topographic image of a 200-nm-wide NiFe/Cu/Co nanowire. (b) XMCD-PEEM image of the magnetic domain structure in the NiFe layer after application of a strong field $H$ transverse to the principal axis of the zigzag. (c) Schematic view of the electronic circuit used for applying and monitoring the current pulses.

The domain structure in the NiFe layers has been observed by XMCD-PEEM at the European Synchrotron Radiation Facility (beamline ID08) and at the Synchrotron SOLEIL (beamline TEMPO). Both magnetic and current pulses could be applied to the samples. A combination of double stripline like microcoils and a homemade pulsed current supply was used to produce the field pulses.[28] The magnetic field is used for saturating the magnetization in the straight sections of the nanowire or to reinitialize a multidomain state prior to applying current pulses. Current pulses were injected using a fast pulse generator providing voltage pulses with a 0.2 ns risetime and a tunable length, ranging from 0.5 to 12 ns. The actual current flowing through the nanowires was deduced from the voltage measured across the 50 Ω input impedance of a 6 GHz oscilloscope connected in series with the nanowires (Fig. 1).

Note that the current densities reported in this work are calculated from the measured voltages assuming an inhomogeneous current distribution in the trilayer. Calculations based on the Fuchs-Sondheimer model[29,30] show that only around 10% of the total current flows in the NiFe layer. The current-density values are approximately two times lower than those obtained assuming a homogeneous current distribution.

During the experiments, the voltage on the objective lens of our Focus IS-PEEM was kept at 4–4.2 kV, in order to avoid discharges onto the sample. This limits the spatial resolution to about 0.6 $\mu$m.[11] Even though the DW shape is convoluted with the resolution Gaussian, the relative change in the DW position can be detected with an accuracy of about 30 nm. In order to image the domain structure in the NiFe layer, the x-ray energy was tuned to the Ni $L_3$ absorption edge (852.8 eV). To optimize the magnetic contrast, the difference between two consecutive images obtained with 100% left- and right-circularly polarized x rays was com-

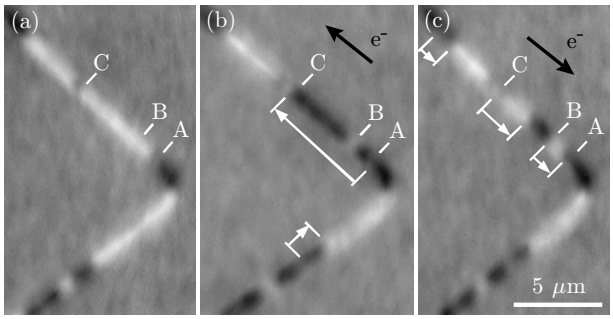


FIG. 2. (a) Initial-state domain structure obtained for a 200-nm-wide nanowire by applying a magnetic field pulse. DW structure obtained after the application of 10-ns-long current pulses with an amplitude of $4.2\times10^{11}$ A/m$^2$ with (b) positive and (c) negative polarities. The DW motion follows the direction of the electron flow. (c) Application of a negative pulse, leading to the displacement B-A, shows DW nucleation at site B.

puted. The presence of a rather thick Cu spacer (8 nm) layer, combined with the limited escape depth of the secondary electrons, prevents the Co domain structure from being imaged. Nevertheless, we were able to obtain information on the magnetization state in the Co layer by studying specific trilayers with a 5 nm Cu spacer. Some complementary images of the Co magnetization state in the samples with 8 nm of Cu were obtained using the high-resolution ELMITEC PEEM at the synchrotron ELETTRA, after sputtering off part of the NiFe layer. These results will be presented in Sec. II D.

The XMCD-PEEM image contrast is given by the projection of the magnetization on the beam direction [see Fig. 1(b)], i.e., white (black) domains in all the images have their magnetization pointing upwards (downwards), along the nanowires. Note that the images have been all obtained in a quasistatic mode, i.e., after application of a single pulse either of current or magnetic field.

### A. Current-induced DW motion

Figure 2(a) presents a typical NiFe multidomain magnetic configuration obtained after the application of a transverse magnetic field pulse of an amplitude not sufficient to saturate the magnetization of each zigzag section. Application of a 10-ns-long pulse with a current density of $4.2\times10^{11}$ A/m$^2$ leads to a displacement of most of the DWs. As expected for spin-torque-driven motion, the direction of DW motion is determined by the sense of the electron flow, as no magnetic field is applied during the current pulses. The DWs can be moved forth [Fig. 2(b)] and back [Fig. 2(c)] with opposite current polarities, unless the pinning potential is stronger in the final than in the initial position. The DW motion is not symmetric for the opposite polarities, which is often the case in our measurements, as we will show later. The average velocity of a DW can be calculated by dividing the distance traveled by a DW by the corresponding pulse duration. The average velocity of the moving DWs in Fig. 2 ranged from 130 to 240 m/s.

An apparent DW motion against the electron flow was sometimes observed. Every time that this was the case, a region with an intermediate XMCD intensity was observed at the arrival point. These regions, like the one in Fig. 2(c) at position B, can be due to 360° DWs smaller than our experimental resolution (see Sec. II D for a more detailed discussion). A one-directional expansion of such a 360° DW upon application of a current pulse leads to an apparent domain nucleation. Such an apparent domain nucleation at position B in Fig. 2(c) would mean that the displacement A-C in Fig. 2(b) actually consists of two displacements, A-B and B-C. Such "double" displacements were not often observed and have not been taken into account in the statistical analysis of Sec. II C.

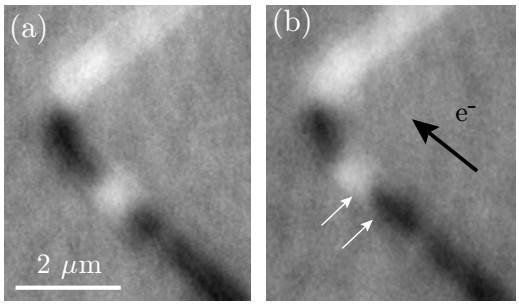


FIG. 3. (a) Initial domain structure obtained with magnetic field pulses before applying current pulses. (b) Head-to-head and tail-to-tail DWs move together upon application of a current pulse (2.5 ns, $3.3\times10^{11}$ A/m$^2$). White arrows indicate the initial position of the DWs.

To prove that the DW motion is governed by spin-transfer torque and not by a residual magnetic field, Fig. 3 shows head-to-head and tail-to-tail DWs moving together.

### B. Determination of pinning strengths

Our previous results[11] already showed that the DWs can move at large velocities for relatively low-current densities, as also seen in Fig. 2, but that the DW motion is strongly hampered by pinning at local-defect positions. Here we support these conclusions by a systematic study showing the effect of magnetic field pulses on the multidomain structure. Figure 4 shows the NiFe domain structure obtained after

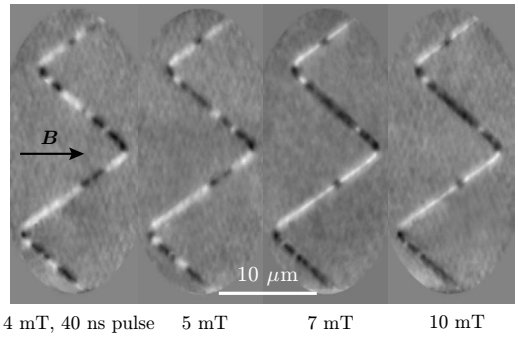


FIG. 4. Measurement of the pinning strength of DWs in a 200-nm-wide nanowire. The NiFe domain structure is imaged after application of one 40-ns-long magnetic pulse of increasing amplitude, going from 4 to 10 mT. The remaining small domains indicate the sites with the largest pinning potentials.

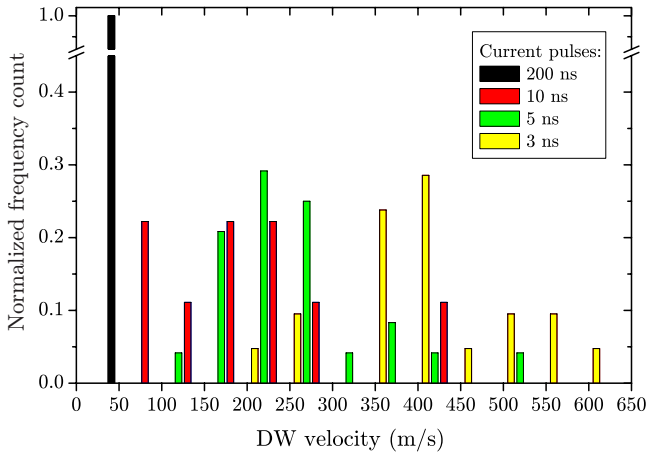


FIG. 5. (Color online) DW-velocity distributions obtained for a 200-nm-wide nanowire using a current density of $3.3 \times 10^{11}$ A/m$^2$ and pulse durations ranging from 3 to 200 ns. The computed velocities for 200 ns pulses all lie in the region below 50 m/s. The columns represent a relative number of events of a given pulse duration in the marked interval (0-50 m/s, 50-100 m/s, etc.)

application of one 40-ns-long magnetic pulse of increasing amplitude. While some domain walls are unpinned by successive field pulses, a complete saturation of magnetization in the individual zigzag sections cannot be reached for the maximum field of our experimental setup. This indicates that the pinning strength at specific positions of the nanowire is larger than 7 mT, i.e., the maximum field used here (10 mT) projected on the direction of the zigzag section. DWs are expected to be pinned at these positions also when spin torque is the driving force for displacement.

### C. Statistics of the current-induced DW motion

The XMCD-PEEM images taken after the application of a single-current pulse of density $2 \times 10^{11}$–$4.2 \times 10^{11}$ A/m$^2$ to an initial multidomain structure show that, in general, some DWs move but also that many others are pinned. Taking into account only the DWs that move for a given current pulse, we have deduced DW displacement and velocity distributions for different pulse lengths and current densities (see Figs. 5–7), starting from many different initial configurations.

Note that these statistical distributions do not describe repeated displacements of the same DWs, but displacements of a multitude of DWs in different parts of the nanowire. This yields a good description of the average behavior of the system, i.e., it is not burdened by a specific pinning potential of a particular DW. DW displacements occurring between the same pinning sites multiple times were removed from the statistical file in order not to influence the distribution.

Figure 5 shows the distributions of DW velocities obtained for a 200-nm-wide nanowire using a current density of $3.3 \times 10^{11}$ A/m$^2$ and different pulse lengths. For each pulse length, approximately 50 events were analyzed. A very large distribution of velocities is obtained, ranging from below 50 m/s to more than 600 m/s. The highest velocities could be achieved only using 3-ns-long pulses. On the contrary, for very long current pulses (200 ns) only low velocities were observed. A direct comparison of the DW motion obtained with a large variety of pulse durations shows that the displacements do not scale with the pulse length and that their values are very close, in general. This strongly suggests that the motion is actually limited by the positions of the pinning sites. This also explains why only by using short pulses we can provide a reliable estimate of the absolute value of the DW velocity.

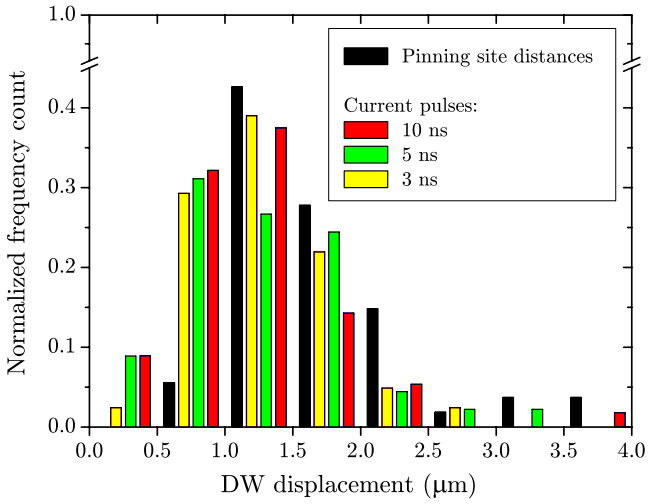


FIG. 6. (Color online) Distributions of DW displacements compared to the distribution of nearest-neighbor pinning site distances in a 200-nm-wide nanowire, obtained for current densities in the range $2 \times 10^{11}$–$4.2 \times 10^{11}$ A/m$^2$. For each pulse length, approximately 50 events were analyzed. The count of displacements is integrated for each marked interval. Note that the spatial resolution of our experiment did not allow determining pinning-site distances smaller than 500 nm, though a relative DW displacement can be determined with a higher precision.

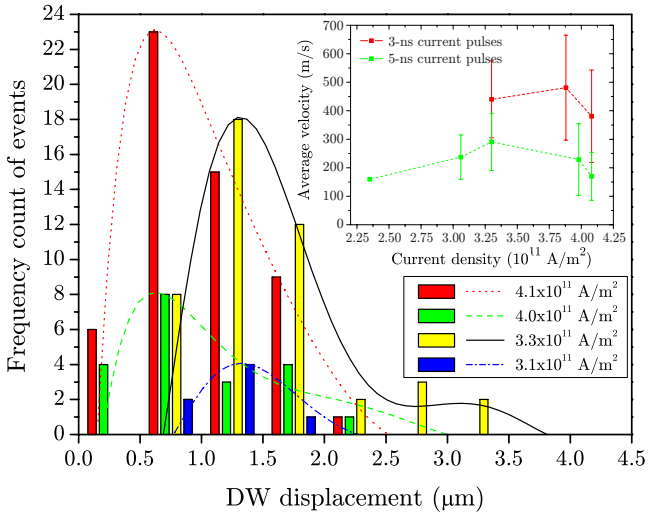


FIG. 7. (Color online) DW displacement distribution in the NiFe layer, induced by current pulses of variable density. The lines are polynomial fits of the displacement distribution for a given current density and represent guides to the eyes. In the inset the dependence of average DW velocity on current density is shown.

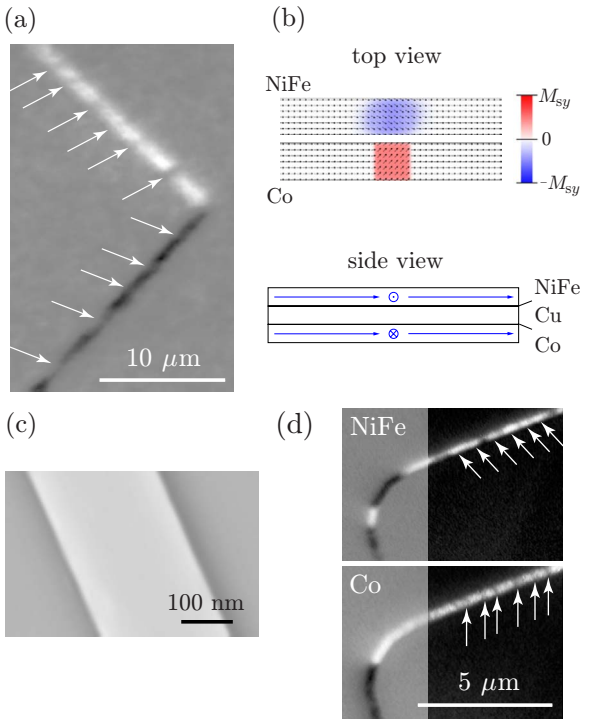


FIG. 8. (Color online) (a) XMCD image of a 200-nm-wide nanowire with magnetization saturated by a transverse field, showing regions of intermediate XMCD intensity associated to DW pinning sites (indicated by white arrows). (b) Micromagnetic simulations showing that a local defect associated to a variation in the Co anisotropy direction induces a local tilt of the NiFe magnetization that reduces the XMCD intensity. (c) Scanning electron microscopy image of the nanowire showing no considerable lateral roughness. (d) High-resolution PEEM images taken for NiFe and Co layers the white arrows indicate the positions of selected gray zones in the Co layer and the corresponding magnetization tilts in the NiFe layer.

In Fig. 6 we compare the integral distributions of current-induced displacements for pulse durations of 3, 5, and 10 ns—including all current-density values—with the distribution of the apparent distances between potential pinning sites, identified as zones with an intermediate XMCD intensity (see Sec. II D). These distances were determined from an image of the saturated magnetic state, like in Fig. 8(a), where the potential pinning sites are indicated by white arrows. A clear correlation exists between the current-induced displacement distributions and the distances between pinning sites, confirming the influence of pinning on the DW motion.

Because of the large pinning probability, DW displacements scaling with the pulse duration were only observed in a few cases and for current pulses shorter than 12 ns. Given the values of the DW velocities and the most probable pinning site distances, it is clear that these events are unlikely: a DW propagating freely at a velocity of 400 m/s moves by 4 $\mu$m in 10 ns; as seen in Fig. 6, there are indeed very few regions of the nanowire where pinning sites are so distant. We emphasize, however, that the occurrence of displacements scaling with the pulse durations is an important proof that the DW moves during the current pulse and not only during the leading and falling edge of the current pulse.[31]

In Fig. 7 we present the dependence of the DW displacement on the applied current density. Though the minimum current density for which we observed DW motion was $2\times10^{11}$ A/m$^2$, only distributions obtained for higher current densities are shown. The average value of the DW displacement first shifts toward higher values as the current increases, but for the highest current values the average displacement decreases. Given the influence of pinning on the DW displacement, especially for long pulses, we emphasize that the shift of the displacement distributions obtained for large current densities was also present when only short pulses of 5 ns were taken into account. Note that the displacements shorter than the minimum measurable pinning site spacing (i.e., less than 500 nm, see Fig. 7) are exclusively induced by current densities higher than $4\times10^{11}$ A/m$^2$. These displacements were obtained for pulse durations of 3 to 10 ns as indicated in Fig. 6.

In the inset of Fig. 7, we display the dependence of the average DW velocity on the injected current density. The DW velocity value was obtained by dividing the average DW displacement by the length of the corresponding current pulse, either 3 or 5 ns. The average DW velocity increases linearly with current density up to $4\times10^{11}$ A/m$^2$. Above $4\times10^{11}$ A/m$^2$, a substantial drop in the average velocity occurs. The large error bars are mainly due the widening of the displacement distributions caused by pinning.

### D. Possible origin of pinning

DW pinning may be induced by structural, topographic, or magnetic defects. In Sec. II A we showed that DWs usually stop and often get blocked for subsequent current pulses, in regions with intermediate XMCD intensities [further called "gray zones," indicated, for example, in Fig. 8(a)]. These gray zones could be induced by features lowering the total x-ray absorption, like artificial defects due to the lithography process or to manipulation of the sample. We discard this possibility, since the corresponding features are generally absent in the sum of the images obtained for right- and left-circular polarizations. The reduced XMCD intensity is thus of magnetic origin. Since the XMCD contrast is proportional to the projection of the local magnetic moment on the incoming photon direction [vertical in Fig. 8(a)], a modified XMCD intensity can be caused by a tilt of the local magnetization away from the easy axis, by a reduction in the local magnetic moment or by domains (360° DWs) smaller than our spatial resolution. In the following, we discuss the different possible sources of DW pinning and their possible relation to the gray zones.

#### *1. Structural and topographic defects*

Structural defects inducing DW pinning could be of intrinsic character, associated to grain boundaries or to a distribution of anisotropy directions among individual grains. However, it is unlikely that these defects act as pinning sites, as the magnetocrystalline anisotropy of NiFe is small and the grain size deduced from transmission electron microscopy images (not shown) is between 5 and 10 nm, much smaller than the minimum measurable DW displacement. Moreover,

similar features were observed for nanowires where the soft magnetic layer was ultrasoft amorphous CoFeB, for which the effect of grain boundaries and magnetic anisotropy should be negligible.

DW may also be pinned by geometrical constrictions in the nanowire[32] or by lateral roughness arising from the lithography process. This mechanism is also unlikely, as the scanning electron microscopy images [Fig. 8(c)] of our nanowires do not reveal substantial lateral roughness. Moreover, the gray zones associated to DW pinning are on average approximately 200–300 nm wide, much larger than the characteristic length of the edge roughness.

### 2. Interlayer dipolar interactions

In SV nanowires, magnetic coupling between NiFe and Co due to the orange-peel interaction associated to rough interfaces might represent a possible source of DW pinning.[33] To check this, we have prepared specific spin-valve samples with optimized interface quality. Using ion-beam-assisted deposition with optimized deposition parameters, we succeeded in strongly decreasing the roughness of the NiFe/Cu/Co interfaces and the magnetic interlayer coupling was almost suppressed.[34] Although the coercive field of NiFe in these samples was decreased, the gray zones were still present in the XMCD images. Interfacial roughness should thus not be at the origin of these gray zones and the associated DW pinning.

Stray fields associated with the presence of DWs or magnetic inhomogeneities in the Co layer are expected to have a strong influence on the local magnetization of the NiFe layer.[2] XMCD-PEEM measurements at the Co $L_3$ edge (779 eV) carried out for a NiFe/Cu/Co spin valve with a 3 nm Cu spacer [see Fig. 9(a)] show that DWs in the Co layer are always and exclusively located at the zigzag corners and are therefore not responsible for the modified contrast in the NiFe layer along the straight sections.

Note, however, that the stray field associated with the Co DWs strongly influences the local domain configuration in the NiFe layer, like it was observed for continuous trilayer films.[35] The domain structure in the NiFe layer near the corners of the zigzag provides a signature of the mutual orientation of the two ferromagnetic layers. If Co and NiFe magnetizations are parallel, the stray field of the Co DW locally reverses the magnetization in the NiFe layer, giving rise to the three DWs shown in the white circle in Fig. 9(b). If Co and NiFe magnetizations are antiparallel, the magnetic flux closes naturally and a single DW is formed [Fig. 9(c)]. This strong coupling prevents current-induced DW motion across the corners in the NiFe layer. This source of DW pinning can be avoided by creating a single domain in the Co layer along the nanowire.

None of the effects mentioned above seems sufficient to explain both the gray zones and the associated DW pinning. Therefore we think that these gray zones are induced by dipolar interactions between NiFe and Co layers. These dipolar interactions will lead to a local tilt in the NiFe magnetization whenever a tilt is present in the underlaying Co layer magnetization, for instance, caused by anisotropy defects. In order to verify this, we have carried out micromagnetic

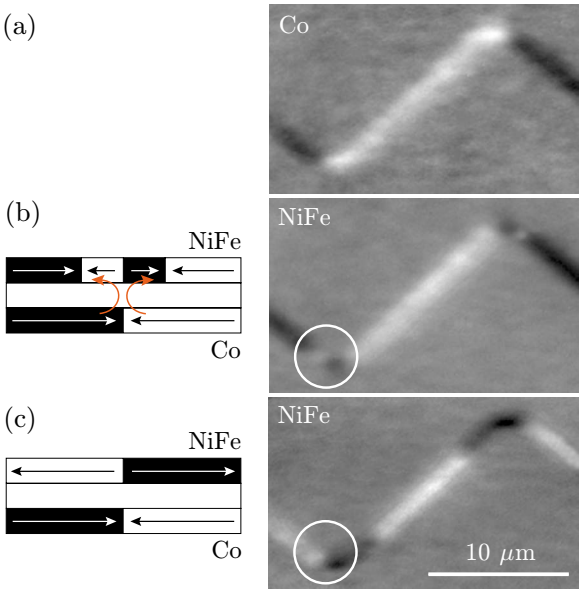


FIG. 9. (Color online) XMCD images of the NiFe and Co layers of a NiFe/Cu(3 nm)/Co trilayer structure, obtained after application of a strong field in the transverse direction. (a) The image taken at the Co $L_3$ edge shows that the DWs in the Co layer are located exclusively at the zigzag corners; in the NiFe, two kinds of domain structures can be found close to the corners, depending on whether the NiFe and Co magnetizations are (b) parallel or (c) antiparallel.

simulations using the OOMMF code.[36] We considered a 200-nm-wide NiFe(5 nm)/Cu(5 nm)/Co(5 nm) spin-valve structure. Both layers were initially uniformly magnetized along the wire direction, except in a $200\times200\times5$ nm$^3$ region of the Co layer where the anisotropy direction is tilted by 45°, within the surface plane. Regions of comparable size consisting of grains with close crystallographic orientations were recently observed by focused ion-beam etching of thin Co films.[37] The system was then allowed to relax under zero applied magnetic field. The following parameters were used in the simulation: spontaneous magnetization $M_S^{NiFe}=800$ kA/m, $M_S^{Co}=1400$ kA/m, exchange constant $A_{ex}^{NiFe}=1\times10^{-11}$ J/m, $A_{ex}^{Co}=3\times10^{-11}$ J/m, and magnetocrystalline anisotropy $K_1^{NiFe}=0$ kJ/m$^3$, $K_1^{Co}=520$ kJ/m$^3$ (as for bulk hcp Co). The cell size was set to $4\times4\times5$ nm$^3$. The results show that the shape anisotropy is not strong enough to overcome the Co magnetocrystalline anisotropy and to align the magnetization within the defect along the nanowire [see Fig. 8(b)]. The stray field associated with the Co defect locally tilts the NiFe magnetization by about 35°. Such a magnetization tilt should strongly modify the XMCD contrast in both layers, as observed in high-resolution PEEM images of a NiFe/Cu(8 nm)/Co nanowire [Fig. 8(d)].

Obviously, the tilt angle of the NiFe magnetization should depend on the value of the magnetocrystalline anisotropy in the Co layer and on the defect volume. However, we found that for a $200\times200\times5$ nm$^3$ defect the magnetization tilt in both layers was not modified upon reducing the magnetocrystalline anisotropy in the Co layer by 1 order of magnitude.

The stray field generated by a defect in the Co layer represents a considerable obstacle for DW motion in the NiFe

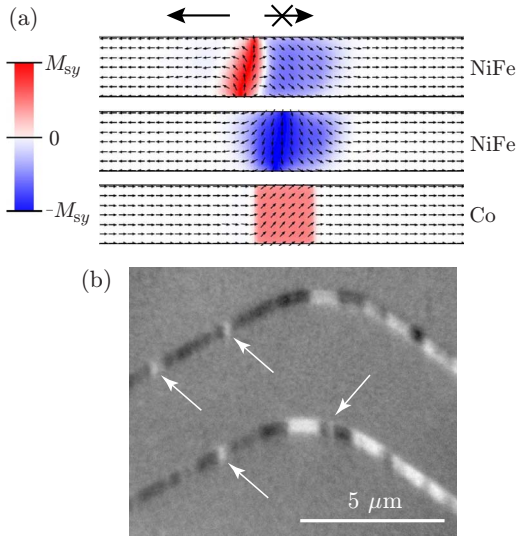


FIG. 10. (Color online) (a) Micromagnetic simulations showing the effect of an anisotropy defect in the Co layer on the mobility of a DW in the NiFe layer. Each sketch represents the top view of the magnetization distribution in Co (bottom) and NiFe (middle and top) layers under the application of a 4 mT magnetic field which drives the DW, initially in the left part of the nanowire, toward the defect. When the magnetization of the NiFe DW is in the same direction as the stray field induced by the Co defect just underneath (middle sketch) the DW is pinned at the defect position. When the Co stray field and the NiFe DW magnetization directions are antiparallel (top sketch) the DW is pushed against the region above the Co defect but cannot be moved across it. However, the DW is free to move away from the defect. (b) High-resolution PEEM images of a 200-nm-wide NiFe/Cu/Co nanowire. The Co images were obtained after removing part of the NiFe layer. White arrows indicate the positions of possible 360° DWs in the NiFe layer.

layer. To illustrate this, we performed micromagnetic simulations in which a TW in the NiFe layer was driven toward the defect under the application of a 4 mT external magnetic field. If the orientation of the transverse component of the stray field and the direction of the magnetization in the NiFe DW are parallel, the DW gets pinned above the Co defect [Fig. 10(a), middle]. In the case of antiparallel alignment [Fig. 10(a), top], the DW cannot even sit atop the Co defect, because of the high-energy cost associated to the dipolar interaction. Thus, whatever the magnetization direction of the DW, a field of 4 mT cannot drive a DW across the region where the Co stray field is present. Similar effects are expected when the DW motion is induced by the electrical current.

When applying current pulses to the NiFe/Cu/Co nanowires, interactions can take place between a DW pinned above a Co defect and a free DW. On one hand, when two DWs of the same chirality approach they can annihilate.[38] In that case, we expect to obtain a gray zone in our XMCD images, at the position where one of the DWs was pinned. On the other hand, if two DWs of opposite chirality approach a 360° DW is formed.[38] Possible 360° DWs can be seen in the high-resolution PEEM images of Fig. 10(b). Because of the limited resolution of the standard IS-PEEM used for the study of DW dynamics, we cannot distinguish between a simple magnetization tilt and such a 360° DW. However, nucleationlike effects at the gray zones can be due to expansion of such a DW.

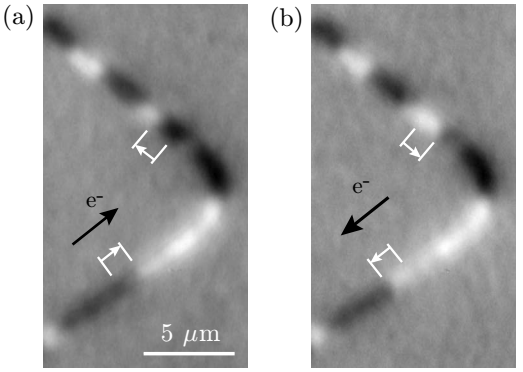


FIG. 11. Reproducible back and forth motions of two DWs between pinning sites using 2.5 ns current pulses of opposite polarity and a current density of $3.5\times10^{11}$ A/m$^2$.

## III. DISCUSSION

Recent studies have shown that the depinning probability of a DW from an artificial defect (like a notch[19,32,39,40] or a bend[41]) in nanowires is highly stochastic, both for field[42,43] and current[22] pulses. The threshold current for DW depinning depends on the shape of the pinning profile[44] and on the temporal shape of the current pulse[45] and can be different for dynamic and static pinning.[46] Considerable domain-wall pinning[22,23,47] can also be induced by natural defects, in which case similar pinning barriers for different defects have been reported.[23] In our spin-valve nanowires, most DWs were depinned within the range of current densities we applied. However, some DWs at particular positions in the nanowire were impossible to move. As discussed above, the most likely origin of this strong DW pinning is the dipolar interaction between the magnetization of the NiFe layer and the anisotropy defects in the Co layer.

Our results clearly indicate that DW pinning is the main drawback for the use of spin-valvelike systems in DW memory applications. Several solutions are now being studied to decrease the pinning. Switching to epitaxial systems might be the solution for obtaining trilayers with fewer defects. It can be foreseen that once pinning will be better understood and controlled and reproducible DW motion will be obtained, spin-valve devices could become a very valuable system for applications. This is demonstrated by the reproducible back and forth motions between two pinning sites that we could obtain many times using 2.5 ns current pulses of opposite polarity and a relatively low-current density ($3.5\times10^{11}$ A/m$^2$) (Fig. 11).

Pinning-limited DW motion may explain ambiguous results reported in the literature for both NiFe and NiFe/Cu/Co systems. When very long pulses are used,[31] the DWs are likely to move only during the first part of the pulse before being pinned, leading to DW displacements not proportional to the pulse length and underestimated DW velocities. Our present study confirms that DW pinning during the pulse has

to be taken into account before discussing the DW dynamics.

One of the obstacles for determining the DW velocity is caused by nucleation and annihilation of domains, which we observed particularly at high-current densities, thus increasing or decreasing the apparent DW velocity. It was theoretically shown that large spin currents applied to a uniform ferromagnet lead to a spin-wave instability resulting in nucleation of magnetic domains.[48] Current-induced domain nucleation was also observed experimentally, by measurements of giant magnetoresistance in SV nanowires[40] and by Lorentz microscopy and electron holography.[49] These studies suggest that good heat dissipation through the substrate is essential. Thomas *et al.*[50] showed that 9 ns pulses with a current density of $5\times10^{11}$ A/m$^2$ applied to spin-valve nanowires deposited on $SiO_2$-coated Si wafers were sufficient to reach the Néel temperature of the antiferromagnetic IrMn (~700 K) which they used for pinning of the hard magnetic layer.

In our measurements, the shape of the current pulse was recorded on an oscilloscope in order to check the effect of current-induced heating on the nanowire resistance. Even for the highest current density we applied, $4.2\times10^{11}$ A/m$^2$ in the NiFe layer ($9.5\times10^{11}$ A/m$^2$ for homogeneous current distribution), we did not observe any decrease in the current amplitude due to heating for current pulses as short as 10 ns.

Recently, we used time-resolved XMCD-PEEM (Ref. 51) to demonstrate that the Oersted field generated by the current flowing in Cu and Co layers of a SV nanowire strongly affects the NiFe magnetization direction during current pulses. Clear changes in the XMCD contrast during the application of a current pulse revealed that the NiFe magnetization tilts by a relatively large angle in the direction transverse to the nanowires. Even if the Oersted field is not specific to SV nanowires,[52] its impact is increased in such devices because of its opposite action on the Co and the NiFe magnetizations. In particular, the dipolar interaction tends to amplify the opposite magnetization tilts initiated in NiFe and Co layers by the Oersted field.

Besides its influence on the quasistatic magnetic configuration in SV nanowires, we also clearly observed that the Oersted field torque affects the magnetization dynamics, by inducing a precession of the magnetization around the effective transverse field.[51] This phenomenon might be responsible for domain nucleation above a threshold current density. This nucleation is most likely to occur at locations where a magnetization tilt in the transverse direction is already present before the current pulse, like at position B in Fig. 2(c). In Ref. 19, a nonexplained reversal of the direction of the DW motion was observed above a certain current threshold value in SV nanowires similar to ours. Our results suggest that this effect could possibly be explained by the nucleation of a domain followed by DW motion in the direction of the electron flow, as proposed in Sec. II A. It is clear that a direct observation of the domain structure and DW motion using magnetic imaging can greatly help understanding the results obtained using magnetoresistance measurements.

An Oersted field might also modify the DW shape resulting in either a widening or a narrowing of the DW. If the DW widens, depinning becomes easier and thus might explain the lower critical-current densities found for SV nanowires[17–19] with respect to single NiFe nanowires.[12,15] The lowest current density for which DW motion was observed in our devices was $2\times10^{11}$ A/m$^2$ for the 200-nm-wide nanowire. This is 3–4× lower than those published for single NiFe nanowires for similar thicknesses and widths of the NiFe layer.[53] For thicker and wider NiFe layers, a decreasing trend of critical-current density has been found.[12] The actual depinning current value is determined by the strength of the individual pinning sites. In our experiments, once depinned, the DWs are able to move at high velocities, showing that we work well above the intrinsic critical density. However, because of the short-pulse length and spatial-resolution limitations, DW motion at very low velocities could not be detected.

In contrast to previous publications where very low values of DW velocities (most probably influenced by the length of the pulses) were reported for single NiFe nanowires,[31] Hayashi *et al.*[15] demonstrated a maximum DW velocity of 110 m/s in 200-nm-wide NiFe nanowires at zero field. This high velocity was obtained for optimized nanowires in terms of DW pinning.[54] In SV nanowires, we find a maximum DW velocity of about $(700\pm20)$ m/s induced by a 3 ns pulse of a current density of $3.9\times10^{11}$ A/m$^2$ and more often velocities in the range of 600–650 m/s. We think that the Oersted field may strongly influence the DW dynamics. Transverse DWs with a magnetization parallel to the Oersted field should be stabilized. This mechanism probably leads to a shift or a suppression of the Walker breakdown and therefore allows high velocities to be reached. This effect is equivalent to that observed for field-induced DW motion, where Glathe *et al.*[55] have shown that application of a transverse magnetic field can considerably increase the longitudinal field for which the Walker breakdown takes place. Micromagnetic simulations including the Oersted field are under progress to confirm this hypothesis. Another specificity of the SV nanowires is the existence of spin accumulation inside the Cu spacer layer in the region of the DW that can give rise to a spin current injected vertically into the DW. This additional channel for the spin transfer from the current to the magnetic moments inside the DW might improve the spin-transfer efficiency, as theoretically shown by Khvalkovskiy *et al.*[20] For a planar polarizer (as in our case) they predict a linear dependence of the DW velocity with the injected current density with velocities above 200 m/s for a current density of $2\times10^{11}$ A/m$^2$. Even if the comparison with our experiments is not straightforward as we inject the current in the film plane, this additional spin-transfer torque due to local-spin accumulation can also contribute to the very large DW velocities. Recently, Boone *et al.*[21] have observed DW velocities up to 800 m/s in the NiFe layer of a SV nanowire by measuring the resonant excitation of a DW in a local pinning potential by a vertical current injection (current density of $J_{ac}=9\times10^{10}$ A/m$^2$). This velocity value, obtained with the current flowing entirely in the direction perpendicular to the multilayer plane, is very close to our observations.

Finally, we discuss the decrease in the average DW velocity observed for current densities above $4\times10^{11}$ A/m$^2$. This decrease could be related to the increase in the total number of DWs that are moving at high-current densities, as we have

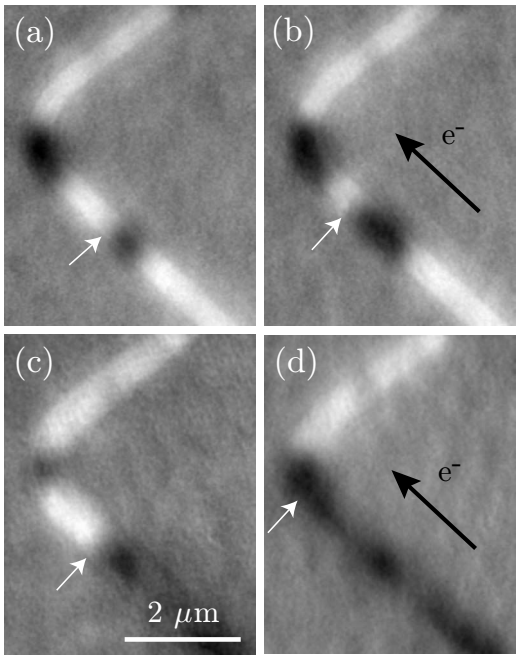


FIG. 12. Domain structures obtained: (a) before and (b) after the application of a 10 ns pulse of a current density of $4.1 \times 10^{11}$ A/m$^2$; (c) before and (d) after the application of a 5 ns pulse of current density $3.1 \times 10^{11}$ A/m$^2$. The displacement induced by the first stronger and wider pulse is shorter than that induced by the subsequent shorter pulse of lower current density. Positions of the DW are indicated by white arrows.

observed in our images. The increased depinning probability of some strongly pinned DWs may give rise to shorter average DW displacements. This hypothesis is contradicted by the observation that some DWs that are mobile at low-current densities move over a substantially shorter distance for current density above $4 \times 10^{11}$ A/m$^2$, as shown in Fig. 12. This suggests that the observed decrease in the DW velocity above a certain current density is real and not an artifact due to the measurement procedure or to pinning restrictions.

The impact of the Oersted field is again probably at the origin of the drop in the DW velocity observed above a certain threshold current density. On one hand, the Oersted field can stabilize the transverse walls, but on the other hand, it induces precession of the DW during its motion which might be a cause for the velocity drop above $4 \times 10^{11}$ A/m$^2$. The Oersted field also leads to a widening of the DW which could result in a lower efficiency of the nonadiabatic component of the spin torque and therefore lead to lower velocities.

## IV. CONCLUSION AND PERSPECTIVES

Using XMCD-PEEM microscopy, we have demonstrated very high velocities for current-induced DW propagation in NiFe/Cu/Co trilayered nanowires with maximum velocities exceeding 600 m/s. These velocities are 4 to 5 times larger than the maximum value reported for other in-plane anisotropy systems.[15] However, we also give clear evidence that the DW motion is strongly hindered by the presence of a large number of pinning sites.

The origin of this higher efficiency of the spin transfer in SV nanowires is most probably manifold. On one hand, vertical spin currents resulting from a local-spin accumulation in the Cu spacer can provide an additional channel for the spin transfer resulting in large DW velocities.[20,21] On the other hand, the exact role of the Oersted field has to be investigated. For example, the Oersted field might increase the depinning probability of a DW with a parallel magnetization and stabilize the DW structure during its motion. However, it can also induce DW widening which might be responsible for a decrease in spin-torque efficiency at high-current densities.

High DW velocities achievable at relatively low current densities make spin-valve systems promising for spintronic devices based on DW displacement. Such trilayers are naturally much more complex than the generally used NiFe systems and for a successful optimization many different aspects, and, in particular, DW pinning, have to be addressed. We have identified several potential pinning sources, among which the dipolar interaction of the NiFe layer with Co anisotropy inhomogeneities is the most probable. This effect remains to be suppressed or controlled in order to be able to discover the full capabilities of the system and to employ it in the future DW devices.

## ACKNOWLEDGMENTS

We acknowledge the technical support of E. Wagner, P. Perrier, D. Lepoittevin, and L. Delrey, as well as the experimental help of S. Pairis, T. Fournier, E. Bonet, W. Wernsdorfer, M. Bonfim, A. Hrabec, S. Laribi, R. Mattana, and C. Deranlot. We are grateful to J. Camarero for discussions and to A. Thiaville for discussions and performing the Fuchs-Sondheimer calculations. E.J. acknowledges financial support through the Acciones Integradas Programme No. HF2007-0071, and Spanish MEC projects No. MAT2006-13470, and No. CSD 2007-00010. V.U. was financially supported by the Grants No. MSM0021630508, No. KAN400100701, No. 2E13800101-MSMT, and by the INGO Project No. LA287 of the Czech Ministry of Education. This work was partially supported by the ANR-07-NANO-034 "Dynawall."

*vojtech.uhlir@uh.cz

[1] G. S. D. Beach, M. Tsoi, and J. L. Erskine, J. Magn. Magn. Mater. **320**, 1272 (2008).

[2] L. Thomas and S. Parkin, in *Handbook of Magnetism and Advanced Magnetic Materials*, edited by H. Kronmüller and S. Parkin (Wiley, New York, 2007).

[3] S. S. P. Parkin, M. Hayashi, and L. Thomas, Science **320**, 190 (2008).

[4] D. Allwood, G. Xiong, C. Faulkner, D. Atkinson, D. Petit, and R. Cowburn, Science **309**, 1688 (2005).
[5] L. Berger, J. Appl. Phys. **49**, 2156 (1978); **55**, 1954 (1984); P. Freitas and L. Berger, *ibid.* **57**, 1266 (1985).
[6] L. Gan, S. H. Chung, K. H. Aschenbach, M. Dreyer, and R. D. Gomez, IEEE Trans. Magn. **36**, 3047 (2000).
[7] S. Zhang and Z. Li, Phys. Rev. Lett. **93**, 127204 (2004).
[8] G. Tatara and H. Kohno, Phys. Rev. Lett. **92**, 086601 (2004).
[9] A. Thiaville, Y. Nakatani, J. Miltat, and Y. Suzuki, Europhys. Lett. **69**, 990 (2005).
[10] T. A. Moore, I. M. Miron, G. Gaudin, G. Serret, S. Auffret, B. Rodmacq, A. Schuhl, S. Pizzini, J. Vogel, and M. Bonfim, Appl. Phys. Lett. **93**, 262504 (2008).
[11] S. Pizzini, V. Uhlíř, J. Vogel, N. Rougemaille, S. Laribi, V. Cros, E. Jiménez, J. Camarero, C. Tieg, E. Bonet, M. Bonfim, R. Mattana, C. Deranlot, F. Petroff, C. Ulysse, G. Faini, and A. Fert, Appl. Phys. Express **2**, 023003 (2009).
[12] L. Heyne, J. Rhensius, Y.-J. Cho, D. Bedau, S. Krzyk, C. Dette, H. S. Körner, J. Fischer, M. Laufenberg, D. Backes, L. J. Heyderman, L. Joly, F. Nolting, G. Tatara, H. Kohno, S. Seo, U. Rüdiger, and M. Kläui, Phys. Rev. B **80**, 184405 (2009).
[13] M. Kläui, P.-O. Jubert, R. Allenspach, A. Bischof, J. A. C. Bland, G. Faini, U. Rüdiger, C. A. F. Vaz, L. Vila, and C. Vouille, Phys. Rev. Lett. **95**, 026601 (2005).
[14] A. Yamaguchi, T. Ono, S. Nasu, K. Miyake, K. Mibu, and T. Shinjo, Phys. Rev. Lett. **92**, 077205 (2004).
[15] M. Hayashi, L. Thomas, C. Rettner, R. Moriya, Y. B. Bazaliy, and S. S. P. Parkin, Phys. Rev. Lett. **98**, 037204 (2007).
[16] N. L. Schryer and L. R. Walker, J. Appl. Phys. **45**, 5406 (1974).
[17] J. Grollier, P. Boulenc, V. Cros, A. Hamzić, A. Vaurès, A. Fert, and G. Faini, Appl. Phys. Lett. **83**, 509 (2003).
[18] S. Laribi, V. Cros, M. Muñoz, J. Grollier, A. Hamzić, C. Deranlot, A. Fert, E. Martínez, L. López-Díaz, L. Vila, G. Faini, S. Zoll, and R. Fournel, Appl. Phys. Lett. **90**, 232505 (2007).
[19] C. K. Lim, T. Devolder, C. Chappert, J. Grollier, V. Cros, A. Vaurès, A. Fert, and G. Faini, Appl. Phys. Lett. **84**, 2820 (2004).
[20] A. V. Khvalkovskiy, K. A. Zvezdin, Ya. V. Gorbunov, V. Cros, J. Grollier, A. Fert, and A. K. Zvezdin, Phys. Rev. Lett. **102**, 067206 (2009).
[21] C. T. Boone, J. A. Katine, M. Carey, J. R. Childress, X. Cheng, and I. N. Krivorotov, Phys. Rev. Lett. **104**, 097203 (2010).
[22] G. Meier, M. Bolte, R. Eiselt, B. Krüger, D.-H. Kim, and P. Fischer, Phys. Rev. Lett. **98**, 187202 (2007).
[23] W. C. Uhlig, M. J. Donahue, D. T. Pierce, and J. Unguris, J. Appl. Phys. **105**, 103902 (2009).
[24] O. Boulle, J. Kimling, P. Warnicke, M. Kläui, U. Rüdiger, G. Malinowski, H. J. M. Swagten, B. Koopmans, C. Ulysse, and G. Faini, Phys. Rev. Lett. **101**, 216601 (2008).
[25] C. Burrowes, A. P. Mihai, D. Ravelosona, J.-V. Kim, C. Chappert, L. Vila, A. Marty, Y. Samson, F. Garcia-Sanchez, L. D. Buda-Prejbeanu, I. Tudosa, E. E. Fullerton, and J. P. Attané, Nat. Phys. **6**, 17 (2010).
[26] V. Uhlíř, N. Rougemaille, O. Fruchart, and J.-C. Toussaint (unpublished).
[27] Y. Nakatani, A. Thiaville, and J. Miltat, J. Magn. Magn. Mater. **290-291**, 750 (2005).
[28] J. Vogel, W. Kuch, J. Camarero, K. Fukumoto, Y. Pennec, M. Bonfim, S. Pizzini, F. Petroff, A. Fontaine, and J. Kirschner, J. Appl. Phys. **95**, 6533 (2004).
[29] E. H. Sondheimer, Adv. Phys. **50**, 499 (2001).
[30] M. Cormier, A. Mougin, J. Ferré, A. Thiaville, N. Charpentier, F. Piéchon, R. Weil, V. Baltz, and B. Rodmacq, Phys. Rev. B **81**, 024407 (2010).
[31] S. Yang and J. L. Erskine, Phys. Rev. B **75**, 220403(R) (2007).
[32] M. Hayashi, L. Thomas, C. Rettner, R. Moriya, X. Jiang, and S. S. P. Parkin, Phys. Rev. Lett. **97**, 207205 (2006).
[33] L. Néel, C. R. Acad. Sci. **255**, 1676 (1962).
[34] V. Uhlíř, M. Urbánek, L. Ranno, P. Bábor, A. Masseboeuf, P. Bayle-Guillemaud, J. Spousta, and T. Šikola (unpublished).
[35] J. Vogel, S. Cherifi, S. Pizzini, F. Romanens, J. Camarero, F. Petroff, S. Heun, and A. Locatelli, J. Phys.: Condens. Matter **19**, 476204 (2007).
[36] M. J. Donahue and D. G. Porter, NIST Interagency Report No. NISTIR 6376, 1999 (unpublished).
[37] M. Urbánek, V. Uhlíř, P. Bábor, E. Kolíbalová, T. Hrnčíř, J. Spousta, and T. Šikola, Nanotechnology **21**, 145304 (2010).
[38] D. Djuhana, H.-G. Piao, S.-C. Yu, S. K. Oh, and D.-H. Kim, J. Appl. Phys. **106**, 103926 (2009).
[39] M. Tsoi, R. E. Fontana, and S. S. P. Parkin, Appl. Phys. Lett. **83**, 2617 (2003).
[40] Y. Jang, S. Yoon, K. Lee, S. Lee, C. Nam, and B. K. Cho, Nanotechnology **20**, 125401 (2009).
[41] E. R. Lewis, D. Petit, L. Thevenard, A. V. Jausovec, L. O'Brien, D. E. Read, and R. P. Cowburn, Appl. Phys. Lett. **95**, 152505 (2009).
[42] M.-Y. Im, L. Bocklage, P. Fischer, and G. Meier, Phys. Rev. Lett. **102**, 147204 (2009).
[43] J. Briones, F. Montaigne, D. Lacour, M. Hehn, M. J. Carey, and J. R. Childress, Appl. Phys. Lett. **92**, 032508 (2008).
[44] S. Lepadatu, A. Vanhaverbeke, D. Atkinson, R. Allenspach, and C. H. Marrows, Phys. Rev. Lett. **102**, 127203 (2009).
[45] L. Bocklage, B. Krüger, T. Matsuyama, M. Bolte, U. Merkt, D. Pfannkuche, and G. Meier, Phys. Rev. Lett. **103**, 197204 (2009).
[46] S.-M. Ahn, K.-W. Moon, D.-H. Kim, and S.-B. Choe, Appl. Phys. Lett. **95**, 152506 (2009).
[47] G. Nahrwold, L. Bocklage, J. M. Scholtyssek, T. Matsuyama, B. Krüger, U. Merkt, and G. Meier, J. Appl. Phys. **105**, 07D511 (2009).
[48] J. Shibata, G. Tatara, and H. Kohno, Phys. Rev. Lett. **94**, 076601 (2005).
[49] Y. Togawa, T. Kimura, K. Harada, T. Akashi, T. Matsuda, A. Tonomura, and Y. Otani, Jpn. J. Appl. Phys., Part 2 **45**, L1322 (2006).
[50] L. Thomas, M. Hayashi, X. Jiang, C. Rettner, and S. S. P. Parkin, Appl. Phys. Lett. **92**, 112504 (2008).
[51] V. Uhlíř, S. Pizzini, N. Rougemaille, V. Cros, E. Jimenez, L. Ranno, O. Fruchart, M. Urbanek, G. Gaudin, J. Camarero, C. Tieg, F. Sirotti, and J. Vogel, arXiv:1002.1302 (unpublished).
[52] D. Morecroft, I. A. Colin, F. J. Castaño, J. A. C. Bland, and C. A. Ross, Phys. Rev. B **76**, 054449 (2007).
[53] N. Vernier, D. A. Allwood, D. Atkinson, M. D. Cooke, and R. P. Cowburn, Europhys. Lett. **65**, 526 (2004).
[54] M. Hayashi, L. Thomas, R. Moriya, C. Rettner, and S. S. P. Parkin, Science **320**, 209 (2008).
[55] S. Glathe, R. Mattheis, and D. V. Berkov, Appl. Phys. Lett. **93**, 072508 (2008); S. Glathe, I. Berkov, T. Mikolajick, and R. Mattheis, *ibid.* **93**, 162505 (2008).